AD-A234 267

TATION PAGE

Form Approved
OMB No. 0704-0188

2. Report Date.	3. Report Type and Dates Covered.
1991	Journal Article

4. Title and Subtitle.
Fram Strait Satellite Image-Derived Ice Motions

5. Funding Numbers.
63704N
Program Element No
X1596
Project No
100
Task No
DN394464
Accession No

6. Author(s).
J. Hawkins and R. H. Preller

7. Performing Organization Name(s) and Address(es).
Naval Oceanographic and Atmospheric Research Laboratory
Ocean Science Directorate
Stennis Space Center, MS 39529-5004

8. Performing Organization Report Number.
JA 321:066:89

9. Sponsoring/Monitoring Agency Name(s) and Address(es).
Space and Naval Warfare Systems Command
Washington, DC

10. Sponsoring/Monitoring Agency Report Number.
JA 321:066:89

11. Supplementary Notes.
JGR

12a. Distribution/Availability Statement.
Approved for public release; distribution is unlimited.

12b. Distribution Code.

13. Abstract *(Maximum 200 words)*.

In order to develop an operational method for the U.S. Navy/NOAA Joint Ice Center to extract ice velocity vectors from sequential advanced very high resolution radiometer (AVHRR) imagery, we have combined the maximum cross correlation (MCC) method with a spatial filtering technique on the image inferred ice motion vectors. We compute the cross correlations between images directly from the image brightness values rather than computing FFTs. The direct method allows greater flexibility in computational parameter settings and allows one to compute motion vectors near coastlines where irregular windows are required. By using a combination of statistical and spatial filters we can then retrieve coherent ice motion vectors in the presence of cloud contaminated imagery. A series of six satellite images of the Fram Strait region, from April 1986, was used to compute sea ice motion from pairs of sequential images. The resulting ice motion vectors were taken as a representation of the surface flow field derived objectively from the satellite imagery. Resulting vector motion fields were found to match well with manually tracked vectors for the same images, thus verifying the validity of the objective MCC method of computing ice motion. These techniques were applied to both the visible and infrared AVHRR channels and to images with different spatial resolutions yielding an overall bias accuracy of about 0.5 cm/s and standard deviations of about 0.9 cm/s. The MCC ice motion results were also compared with wind-driven numerical model were thought to be primarily due to a stronger ocean current than was present in the model.

14. Subject Terms.
(U) Sea Ice; (U) Lead; (U) Texture

15. Number of Pages.
18

16. Price Code.

17. Security Classification of Report.	18. Security Classification of This Page.	19. Security Classification of Abstract.	20. Limitation of Abstract.
Unclassified	Unclassified	Unclassified	SAR

volume 96
number C3

MARCH 15, 1991

JGR

Journal of Geophysical Research

PUBLISHED BY AMERICAN GEOPHYSICAL UNION

Including Special Section:
Marginal Ice Zone Experiment III

JOURNAL OF GEOPHYSICAL RESEARCH, VOL. 96, NO. C3, PAGES 4751–4768, MARCH 15, 1991

Fram Strait Satellite Image-Derived Ice Motions

W.J. EMERY AND C.W. FOWLER

Colorado Center for Astrodynamics Research, University of Colorado, Boulder

J. HAWKINS AND R.H. PRELLER

National Oceanographic and Atmospheric Research Laboratory, Stennis Space Center, Mississippi

In order to develop an operational method for the U.S. Navy/NOAA Joint Ice Center to extract ice velocity vectors from sequential advanced very high resolution radiometer (AVHRR) imagery, we have combined the maximum cross correlation (MCC) method with a spatial filtering technique on the image inferred ice motion vectors. We compute the cross correlations between images directly from the image brightness values rather than computing FFTs. The direct method allows greater flexibility in computational parameter settings and allows one to compute motion vectors near coastlines where irregular windows are required. By using a combination of statistical and spatial filters we can then retrieve coherent ice motion vectors in the presence of cloud contaminated imagery. A series of six satellite images of the Fram Strait region, from April 1986, was used to compute sea ice motion from pairs of sequential images. The resulting ice motion vectors were taken as a representation of the surface flow field derived objectively from the satellite imagery. Resulting vector motion fields were found to match well with manually tracked vectors for the same images, thus verifying the validity of the objective MCC method of computing ice motion. These techniques were applied to both the visible and infrared AVHRR channels and to images with different spatial resolutions yielding an overall bias accuracy of about 0.5 cm/s and standard deviations of about 0.9 cm/s. The MCC ice motion results were also compared with wind-driven numerical model simulations of the region. Marked differences between the MCC image-derived velocities and those from the numerical model were thought to be primarily due to a stronger ocean current than was present in the model.

INTRODUCTION

Satellite image data are a valuable source of information on the temporal changes of sea ice surface conditions. The difficulty of collecting in situ data in Arctic regions along with the problem of directly measuring sea ice displacements makes satellite imagery an attractive source of ice motion data and increases the value of quantitative information derived from these imagery. A series of visible, infrared, or synthetic aperture radar (SAR) images monitors the positions of ice floes at particular times, and movements of sea ice can be computed as displacements between the images. By manually following obvious features of the pack ice in these sequential images, it is possible to derive the field of ice motion vectors [*LaViolette and Hubertz*, 1975]. Such a subjective "feature tracking" technique is very labor intensive and requires large amounts of operator time to locate the image features in the successive images and compute the displacement vectors. This method also suffers from the limitation that it is difficult to clearly identify the same features in each image pair because of changes in brightness due to partial cloud cover, surface roughness changes, ice deformation, etc.

An automated technique for computing ice motion from sequential imagery was first described by *Ninnis et al.* [1986]. Similar to the technique developed for the automated tracking of clouds in satellite imagery [*Leese et al.*, 1971; *Schmetz and Nuret*, 1987], our method locates the maximum cross correlations (MCC) between sequential images as the end points of vectors in windowed portions of the images. Applied to visible imagery from the advanced very high resolution radiometer (AVHRR) with a spatial resolution of about 1 km, this method produced reasonable maps of sea ice motion for pairs of images from the Beaufort Sea region [*Ninnis et al.*, 1986]. Comparisons with wind derived ice motions indicated that the magnitude of the MCC vectors was consistent with wind-driven ice movements.

Subsequent studies [*Fily and Rothrock*, 1987; *Vesecky et al.*, 1988; *Collins and Emery*, 1988] applied this same technique to image pairs from a synthetic aperture radar. The higher spatial resolution (10 to 100 m) and all-weather sensing capability available with SAR data produced detailed maps of the ice floes imaged in the data. The objective MCC method takes maximum advantage of this higher spatial detail, yielding greater resolution in the vector ice motion fields without the added time for operator interaction.

In the present study the MCC method is applied to a series of AVHRR imagery from the Fram Strait region. Both near-infrared (AVHRR channel 2) and thermal infrared (AVHRR channel 4) imagery were utilized to compute sea ice motion in order to establish similarities and differences in the use of these different channels. In subsequent sections we discuss a series of statistical and spatial coherency filters, developed to automatically remove erratic motion vectors due to cloud contamination and other nonadvective causes. After filtering,

Paper number 90JC02273.
0148-0227/91/90JC-02273$05.00

the resulting motion fields are compared with similar motion computations made with a wind-driven ice model [*Preller and Posey*, 1989]. In the summary section, recommendations are made for the application of the MCC method and the filter techniques to the routine operational computation of sea ice motion.

DATA

The AVHRR imagery used in this study were from April 19 - 25, 1986, as more fully detailed in Table 1. This set of images was chosen due to their exceptionally cloud-free conditions. The data were acquired via the Satellite Digital Receiving and Processing System (SDRPS) at the Naval Ocean Research and Development Activity [*Hawkins et al.*, 1985]. This facility collected 1-km local area coverage (LAC) image data. The satellite images were navigated to a polar stereographic projection of 1024 by 1024 pixel images. After navigation, each image pixel is about 1.1 km square across the entire image. Thus all computations were carried out in pixel space with no special corrections needed for pixel stretching with latitude (the error is about 1% between top and bottom of the image).

TABLE 1. Fram Strait AVHRR Images

Image	Date	Time (UT)
1	April 19, 1986	1535
2	April 21, 1986	1510
3	April 22, 1986	1459
4	April 23, 1986	1448
5	April 24, 1986	1256
6	April 25, 1986	1305

The precise location of each image, after navigation was adjusted using a separate registration to preselected ground control points (GCP). This final registration accounts for image registration errors due to the incorrect time of collection, satellite attitude variations, etc. The GCP corrections are done by hand using obvious landmarks such as points and bays to insure the accurate locations of each pixel, an obviously stringent requirement of the MCC method. Any mislocation in pixel navigation will lead to errors in both the MCC computed motion vectors and those derived by feature tracking. In addition both images must be navigated to the same accuracy and are coregistered. GCP correction reduced the typical location errors from 2-4 pixels to a single pixel.

A 1-km pixel error in each image can contribute a ±2 km error in the image-pair-derived MCC location which converts to an approximately 2.54-cm/s error for a 24-hour separation between images. In our images the study area has a comparatively large amount of cloud free land, making good image coregistration possible. Images in the central Arctic Ocean would present a problem: little land exists for image registration, and even a 1-pixel image location error could lead to a 50% error in the velocity computation, since ice motions are small and often erratic on a short time period.

Both channel 2 (near-infrared, 0.73-1.1 μm) and channel-4 (thermal infrared, 10.3-11.3 μm) images were used to compute MCC ice motion vectors. During the Arctic summer, light conditions are such that visible channels can be used to compute MCC displacements, but in winter only the thermal infrared channel is available for imaging the sea ice movements. Thus it is important to understand the application of the MCC method to both visible and thermal infrared imagery.

The 10-bit brightness values of the AVHRR channels were converted to eight-bit gray shades, optimized for the narrow range of values relevant to ice imagery. The six images selected for this study were exceptional not only for their low cloud cover amount, but also for displaying large portions of the pack ice and the marginal ice zone. Later it was found that there was contamination from low clouds that were filtered out by statistical and spatial filtering techniques. No simple cloud mask technique, either single-channel or multichannel, proved to be adequate for an a priori removal of these subtle cloud signatures. Instead, we found it to be more effective to filter the resulting motion fields themselves to remove the cloud contamination. Since cloud motions are spatially less coherent than those of the pack ice field, the directional variability of the motion field provided a good mechanism for filtering out the cloud contaminated motion vectors.

Examples of the images used in this study are given in Figure 1 and Figure 2. These are channel 4 AVHRR images with a coastal outline map and a latitude, longitude map superimposed on them for reference. Higher ice concentrations are indicated by the brighter gray shades and leads appear as darker lines in the pack ice. Off to the east (Figure 1), streaks of high cloud can be seen as even whiter shades which cover most of Spitsbergen. Clouds are also apparent in Figure 1 over the northeast coast of Greenland. There is in general less cloud cover in the second image (Figure 2) with only a few streaks indicating the presence of high clouds. It should be noted that clouds can be recognized in the imagery by their texture, which appears fuzzy compared with the more distinct ice surface patterns.

These images are essentially 24 hours (Table 1) apart and the advective changes that are detected by the MCC method are very difficult to observe by visual inspection of the images. By concentrating on individual ice floes it is possible to see a general southward pack ice movement through the Fram Strait. The black vectors superimposed on these images were computed with the MCC method for this 24-hour image pair.

MCC METHOD IMPROVEMENTS

The goal of the MCC method is to develop a completely objective method for computing ice motion from sequential AVHRR imagery. The core concept of the method is that the maximum cross correlations, in windowed portions of the satellite images, can be taken as the end points of motion vectors that originate at the center of the window in which the search for the maximum correlation is carried out [*Ninnis et al.*, 1986] Rather than the Fourier transform technique used in the earlier study, we computed the cross correlations directly in order to have flexibility in the spatial resolution. The Fourier technique requires a constant, rectangular computational domain, with sizes that are powers of 2 for the fast fourier transform (FFT), which is impossible to maintain if any masking is required (i.e., land or cloud). With the direct approach we can decrease the size of the search windows adjacent to the coast to accommodate the geographic boundary.

In our application of the direct cross correlation computation we have removed all land pixels from the search windows with a land mask. The remaining image pixels are then used to

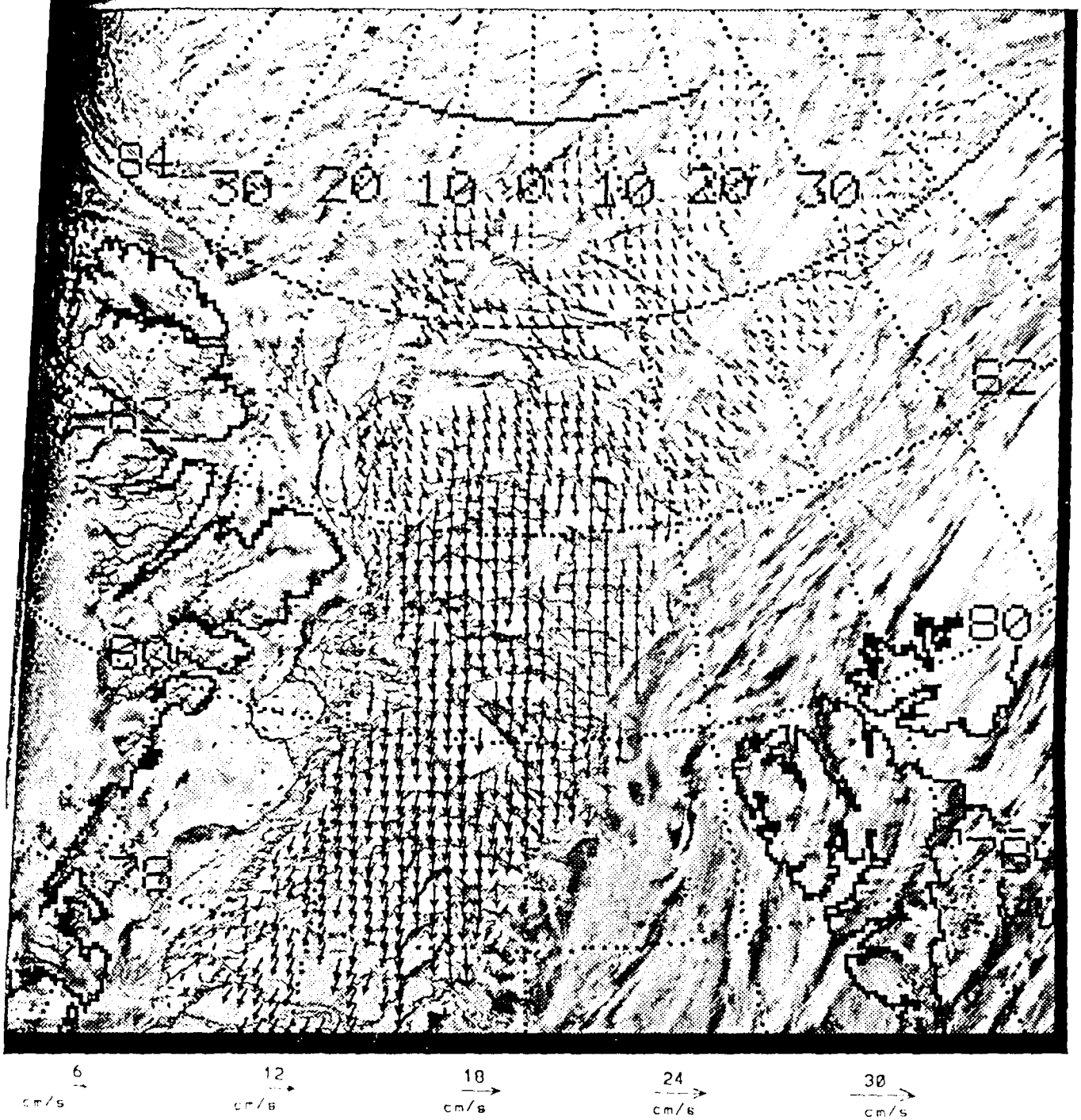

Fig. 1. Channel 4 AVHRR image of the northern Fram Strait, April 22, 1986, with the motion vectors overlaid that were computed from Images 1 and 2. The vector velocity scales are given at the bottom of the image.

compute the cross correlations. This same a priori filtering can also be used for cloud masking. For example, if a multichannel cloud detection scheme is implemented, a cloud mask can be defined and the cloudy pixels flagged so as not to be used in the MCC computation. This type of filtering would not be possible with the FFT method, since all of the pixel values in the search and template windows have to be used to compute the cross correlations. Thus the direct method has definite advantages that can outweigh any FFT speed advantage depending on the application.

There is, however, a limit at which the pixels remaining in the search window are considered to be too few for an accurate MCC computation. For this study we set this level at 60% of the total pixels in the window; this means that for a 15 by 15 pixel template window 135 points must be available to compute the cross correlations before the window will be included in the vector field. The degrees of freedom available with 135 pixels is more than enough to provide the statistical significance required in the MCC computation. Statistical significance level provides one way of eliminating some of the

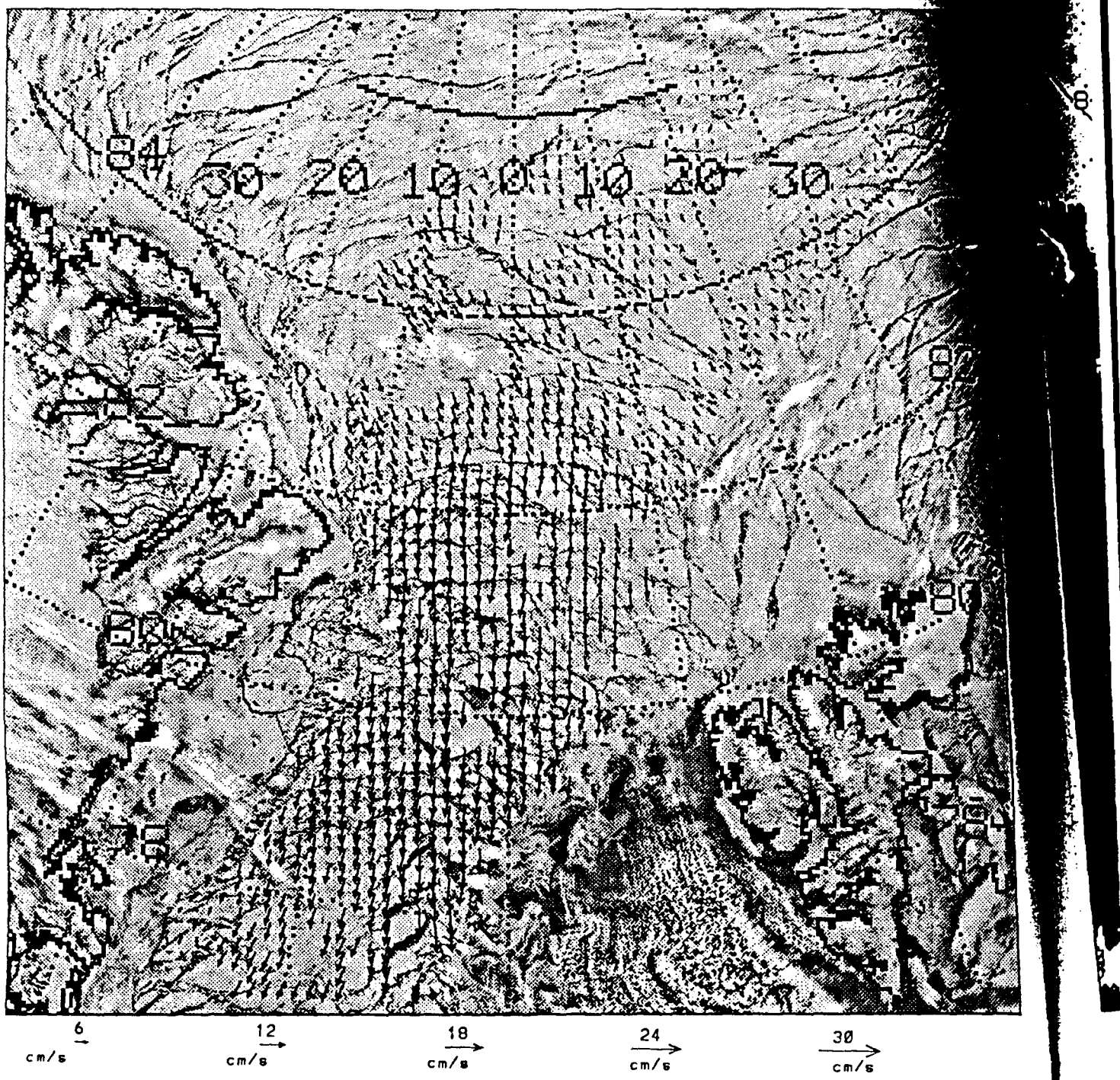

Fig. 2. As in Figure 1 for April 23, 1986; the second image in the pair used to compute ice motion for this period.

less spatially coherent vectors because of their lack of statistical significance in the computation of the MCC.

Another addition to the earlier MCC computational technique [*Ninnis et al.*, 1986] is that we overlapped search windows to compute a much tighter spatial grid of output motion vectors. This change provides a much smoother vector motion field from the image pair without the need to do a separate grid interpolation; this method instead uses the image correlations themselves to perform the spatial interpolation. This reduces the statistical integrity of the vector field in that each vector is no longer completely independent of its neighbors. The benefits of the smooth spatial fields can outweigh any likely limitations created by the lack of statistical independence. It should be pointed out that any other form of interpolation would also reduce statistical independence.

An important facet of the MCC technique is the choice of the search windows. The search window is that portion of one image within which the maximum cross correlation is computed by moving about a smaller template window from the other image in the sequential pair. The overall size of this search window, along with the interval between the images, sets the magnitude of the ice velocities that can be resolved by the MCC

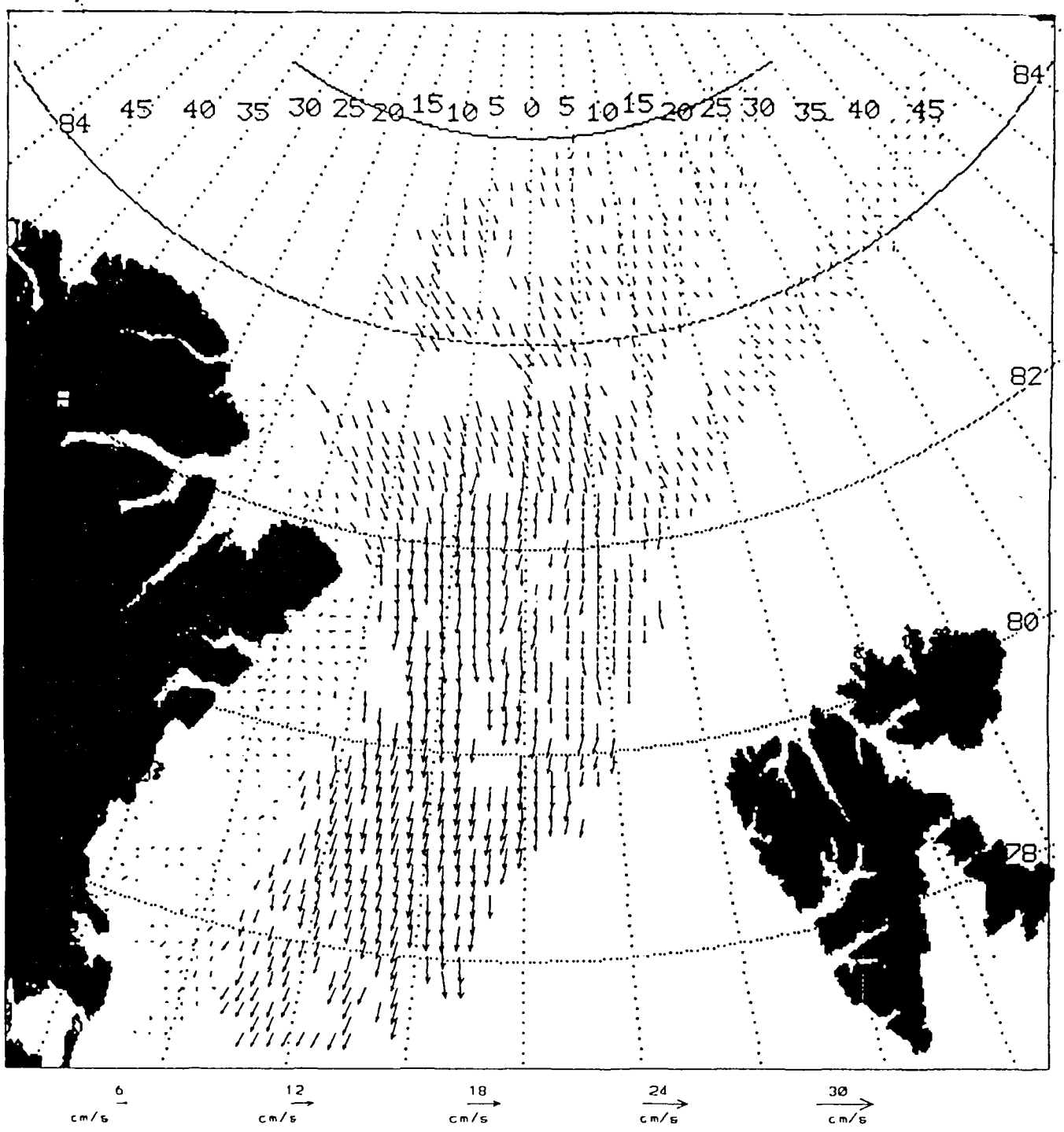

Fig. 3. MCC computed and filtered ice motion velocities for the images in Figure 1 and Figure 2.

computation. For our series of Fram Strait images we assumed a typical maximum speed of about 30 cm/s and selected 55 by 55 pixel search windows and 15 by 15 pixel template windows. The locations of the maximum correlations in the search windows are taken to be the end points of motion vectors having their origins at the centers of the search windows. The pixel template window size also depends on the assumption that the ice motion is piecewise linear. There is a trade-off between using too small a box size (lack of statistical significance) and using too large a window size that misses the smaller ice motions.

Ice motions were computed with the MCC method for all AVHRR images in the series described above. An example can be seen in Figure 3 which shows the ice motion vectors computed from the images of Figure 1 and Figure 2. This same set of ice motion vectors is superimposed on the images in Figure 1 and Figure 2 to give a better feel for the ice features being tracked by the MCC method. The dominant flow is southward through Fram Strait with ice velocities ranging from 5 to 15 cm/s (note speed scale at the bottom of the figure). Weaker velocities are found to the north of the Strait where the ice feeds into Fram Strait. Clear funneling of the ice from the

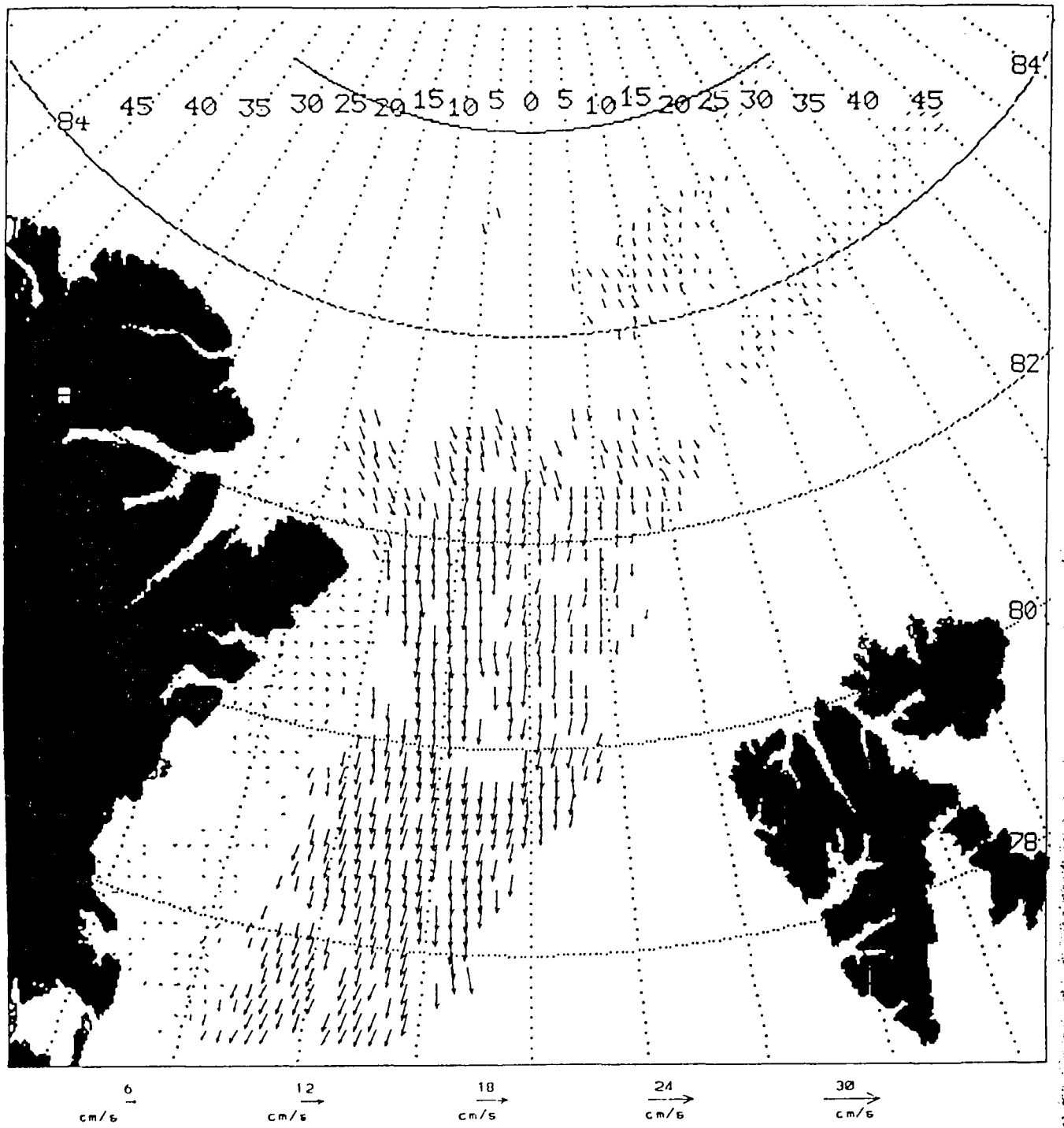

Fig. 4. Unfiltered MCC velocities (cutoff of 0.1) computed from the images in Figure 1 and Figure 2.

west into Fram Strait can be seen in these vectors. Clouds have been filtered out using methods that will be described in subsequent sections. Cloud removal has created the gaps at the northern and eastern limit of this vector field. At the western edge, the zero velocity vectors represented by dots, indicate the lack of motion in the shore fast ice.

In those regions where the ice pack is breaking up, there are many individual ice floes which are not following the general ice pack. In its present form, the MCC method assumes a linear displacement from one image to the next. Thus it is incapable of resolving floe rotations and deformations that predominate in the marginal ice zone.

FILTER TECHNIQUES

We have already presented filtered results of the MCC computation for the channel 4 AVHRR images on April 22 and 23 in Figure 3. To understand how this field of vectors was produced, we show Figure 4, the field of all vectors that were computed for this same image pair of 1024 by 1024 pixel

ages. The resulting field of vectors reveals the strong herent ice motion pattern in the central portion of the field d many spatially incoherent vectors on the borders. There a number of spurious vectors scattered across the central, herent-motion section as well. Most of the spatially oherent vectors have velocity magnitudes equal to or greater n the coherent vectors associated with the ice motion.

Two different filters were applied to the vectors of Figure 4 to ld the smooth field in Figure 3. First, a correlation cutoff of , found by *Emery et al.* [1 '86] to be a 95% significance it for similar image data, was applied to all of the MCC lculations. A correlation cutoff value of 0.1 had been used to mpute the full vector field in Figure 4. The use of a higher toff level as a filter, removes vectors that are statistically s significant regardless of their direction. The use of a cutoff el filter accounts for the general noise level of the satellite agery. The relatively low correlation cutoff levels used here lect the relative lack of distinct targets in the ice imagery.

Second, a spatial coherence filter was used that required each ctor to have at least one neighbor that did not deviate in ection more that a single image pixel (essentially, 1 km). r images separated by 24 hours, 1 pixel equates to a 7-cm/s accuracy limit on the ice motion vector. The triction to a single pixel was found to be more useful than other arbitrarily assigned direction limits and is more nsistent with the 1 pixel navigation accuracy of the image ta. The spatially coherent nature of the velocity vectors in gure 3 attests to the success of these filter techniques.

It should be noted that there are some distinct limitations to ese motion filter techniques. For example, if one has a arsely populated field of correct velocities, the nearest ighbor filter would remove most of them due to natural riability across the field itself. Also if a motion field were rongly divergent, the filters could also remove valid velocity ctors. The filter can be changed to be more or less nservative by changing the number of neighboring vectors the amount of deviation allowed for matching. Thus it is cessary to have spatially coherent ice motion (over the time terval between images) for these types of filters to be useful. 'e found that the most effective technique is to first use a rrelation cutoff level to remove most of the image noise duced motion vectors and then apply a spatial filter to remove y residual spurious vectors.

SUBJECTIVE FEATURE TRACKING

In an effort to verify the validity of the MCC motion vectors e same set of satellite images (Table 1) was used with a ndard feature tracking technique to compute the ice motion tween images. This feature tracking was done at the Remote nsing Branch of NORDA on an image processing system hich allowed the operator to select ice features, within any o successive image pairs, and then compute the splacements of these features. The feature tracked splacements were then loaded into an array referenced to the sition in the first image. This technique then produced ctors such as those in Figure 5, which are the velocities tween the images in Figure 1 and Figure 2. Considerable fort was expended to assure that only actual ice features were acked subjectively, eliminating any contributions from cloud uctures.

The subjectively tracked vectors in Figure 5 are very similar the corresponding MCC-computed vectors in Figure 3. The ost striking difference is the abundance of vectors in the MCC velocity field versus the feature tracked version. This is due to the greater effort required with the subjective method. The result is a tendency to reduce the number of features tracked and hence the ice motion field spatial resolution. Both fields exhibit weak (5-10 cm/s) motions off the extreme northeast tip of Greenland, moderate (10-15 cm/s) speeds in the main ice pack near 80°N, and faster (15-20 cm/s) ice motions along the lower concentrations of the marginal ice zone (MIZ).

Similar comparisons were made for all five image pairs in the series and the computed subjective vectors were statistically compared with the most adjacent MCC vectors. A total of 330 vectors were compared as x (east-west) and y (north-south) vector components. The x direction mean difference (bias) was 0.71 cm/s with a standard deviation of 0.62 cm/s. The y direction bias was 0.57 cm/s with a corresponding standard deviation of 0.51. Resolved into overall magnitude the bias was about 1.0 cm/s with a standard deviation of 0.9 cm/s. Compared with general ice velocities of 10-20 cm/s, these differences are quite small (5-10%) and demonstrate the validity of the MCC-derived ice velocities.

COMPARISONS BETWEEN MCC-DERIVED VELOCITIES

A comparison was made between the vectors of Figure 3, computed from channel 4 (thermal infrared) images, and the vectors computed from the corresponding channel 2 images (Figure 6). The vector fields are qualitatively similar with the most apparent difference being the presence of a few additional vectors in the northern part of the channel 4 vector field. It was often found that in the denser part of the pack ice, the channel 4 brightness responded to gray shade differences that were not apparent in the near-infrared channel 2 image of the same region. It may be that leads and other broken areas are covered with a thin reflective surface of new ice which appears in the channel 2 image as continuous, while the thermal emissions, i.e., the flux of heat from the ocean below (R. Holyer, personal communication, 1989), detected by the channel 4 image, may still show the deeper discontinuity that can be followed with the MCC method.

Comparisons between images from other regions, such as the Barents Sea, also demonstrated this same effect with the channel 4 imagery detecting more motion than the equivalent channel 2 images. One note of caution when looking at channel 4 images in summer, is the possibility of very rapid surface temperature changes taking place as meltwater is formed, which can dramatically alter the thermal emissions displayed in the channel 4 image.

Statistical comparisons between the x (east-west) and y (north-south) components of these two vector fields produced virtually identical histograms for both axes. In these histograms, 80% of the 2000 vector pairs were identical, with 19% of the vectors agreeing within 1 pixel (the resolution of the imagery), 1% agreeing within 2 pixels, and no discernible differences beyond 2 pixels. Thus for this pair of images at least, the use of channel 4 or channel 2 AVHRR data yields similar results. It would be interesting to carry out these same comparisons for data later in the spring to see if the effects of summer melt dramatically altered this comparison as suggested above.

Another comparison in MCC methodology was to compare the full resolution vector field in Figure 3 with a similar field computed using a lower spatial resolution channel 4 image. Since AVHRR data are available in two different resolutions, we decided to reduce the 1-km resolution of the images in Figure 1

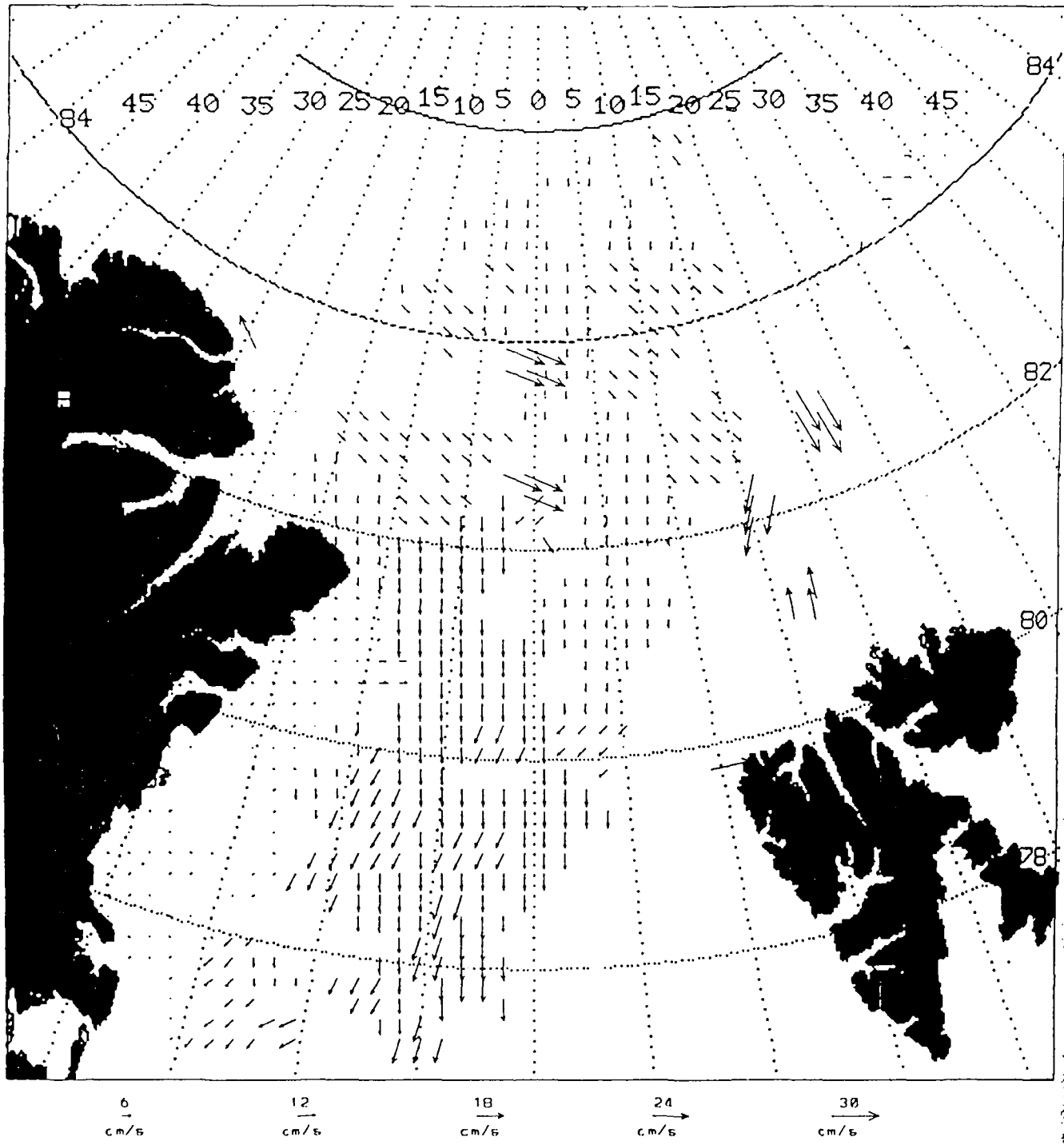

Fig. 5. Feature-tracked (subjective method) ice velocities for the images in Figure 1 and Figure 2.

and Figure 2 with the nominal 4-km resolution available with the AVHRR global area coverage (GAC) data. The vectors in Figure 7 were derived from 4-km images that represent the spatial characteristics of GAC imagery. The overall flow pattern is very similar to that in Figure 3 with the exception of some obvious errors, discussed below.

The subtle changes of the higher resolution flow field are poorly represented, especially where directions vary. The GAC resolution (Figure 7) presents a "blockier" ice motion view than can be seen the in the smooth motion field in Figure 3. It is also important to note that with the poorer spatial resolution, many of the vectors in Figure 3 are lost and a few new, clearly erroneous vectors are introduced. Particularly noticeable are the strong (> 30 cm/s) vectors in the northeast corner which do not appear at all in the higher-resolution version. Some other apparently anomalous vectors appear (Figure 7) in the central pack ice area and are conspicuous by their lack of coherence with the vectors around them.

Comparisons were also made with the image series, between MCC vectors computed over 1-day, 2-day, and 4-day intervals

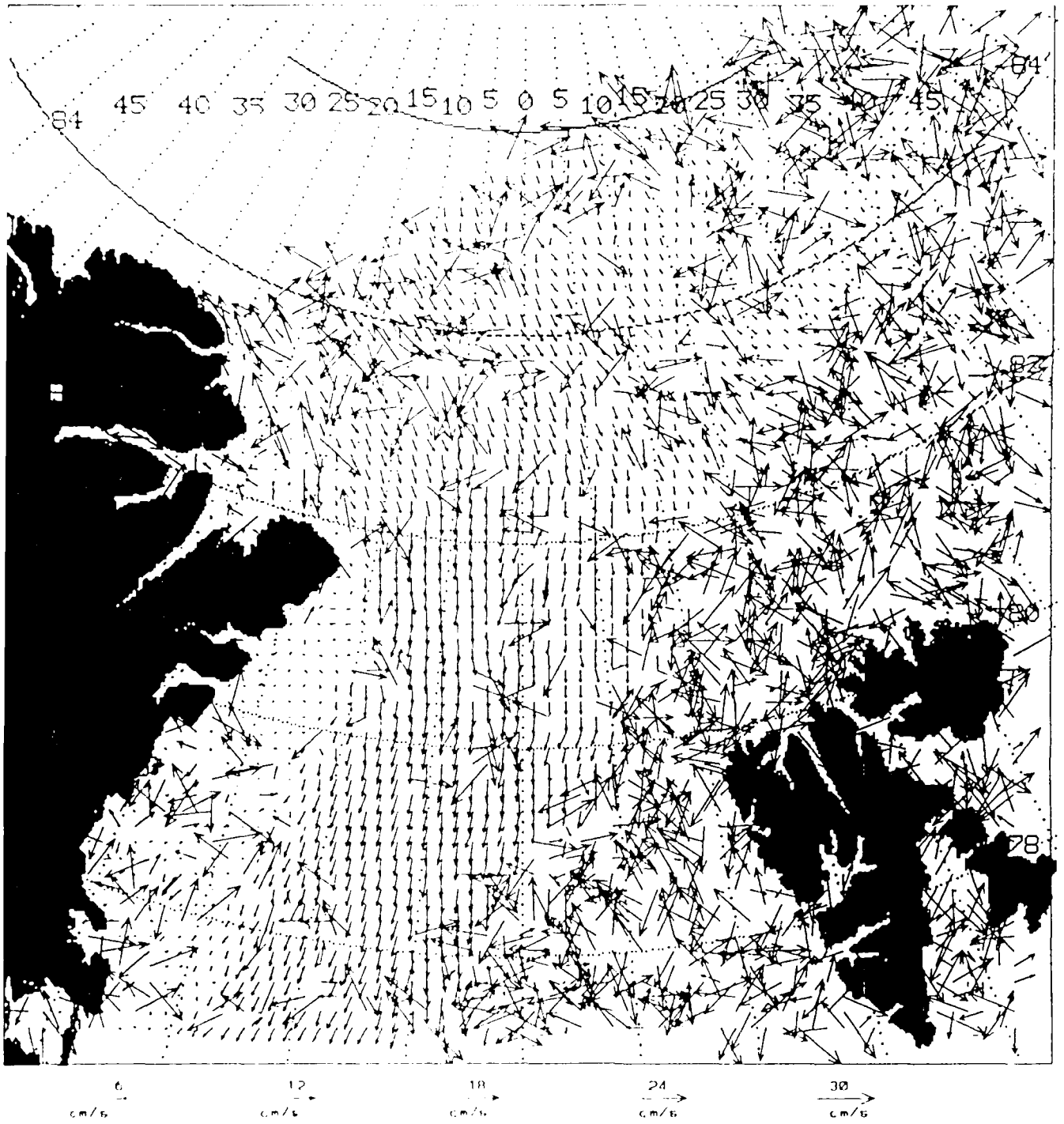

Fig. 6. MCC velocities computed and filtered using the AVHRR channel 2 images corresponding to images in Figure 1 and Figure 2.

between images. The resulting vectors look fairly similar with some differences in overall coverage, due to the various effects of cloud contamination in the different input images used in constructing the image pairs. Histograms of the x and y direction differences, between the 2-day vector field and that generated using images only 1 day apart, are Gaussian in shape with a larger standard deviation in the x direction ($s = 0.48$) than in the y ($s = 0.37$, due to the strong southward flow in Fram Strait). The histograms for the 4-day image interval are smaller in amplitude (on account of the reduced number of vectors available for comparison), but the overall shapes are still Gaussian. The standard deviations are similar to those for the 2-day comparison except that both x and y directions have nearly the same value.

FRAM STRAIT TIME SERIES

Using the same filtering steps applied to produce Figure 3, we computed a time series of motion fields for the six daily images in Table 1. Most intervals between images were a

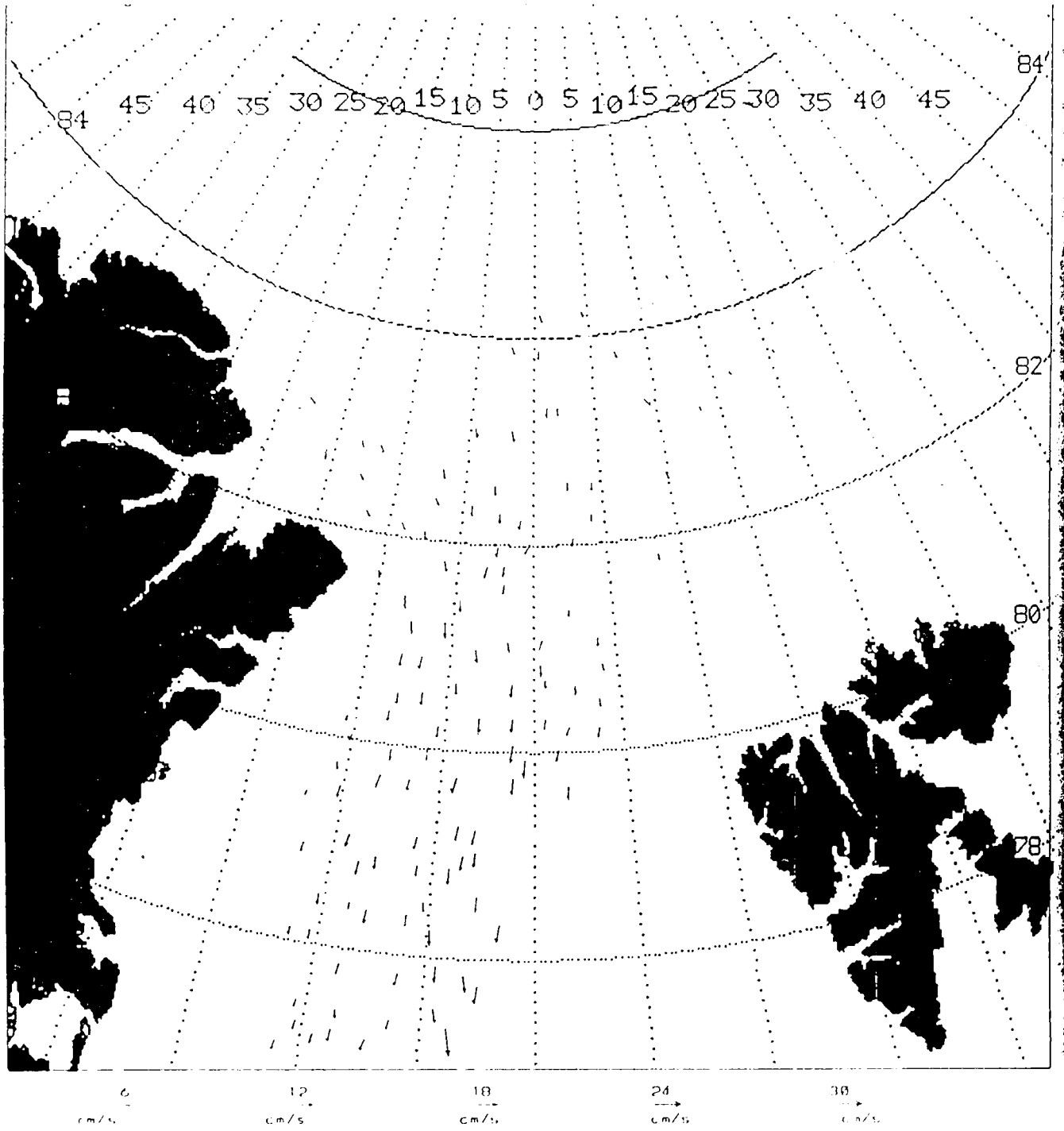

Fig. 7. MCC velocities computed and filtered from reduced 4-km resolution versions of the images in Figure 1 and Figure 2.

single day except for the start of the series where a 2-day gap exists between the first images. Even with this 2-day interval (April 19-21, 1983), however, the resultant MCC motion field in Figure 8*a* appears very coherent. The strong currents in the north central part of the Fram Strait dominate the ice motion with smaller velocities at higher latitudes north of the strait. The pattern of ice feeding into the strait [*Vinje and Finnekaesa*, 1986], particularly from the northwest, is clearly apparent in the image-derived motion vectors and is consistent with traditional flow through a channel.

The image pair between April 21 and 22 was one of the clearest sets of images we have examined. The resulting ice motion field (Figure 8*b*) fills most of the ice covered portion of Fram Strait and the area to the north. Again the greatest ice velocities are in the central strait with strong southward motion through the strait. While ice is again feeding into the strait from the northwest it appears to be exiting f.. the strait on the northeast. This is likely due to a short-term change in the wind field which dominated the prevailing Fram Strait ocean currents and moved the ice in a northeast direction.

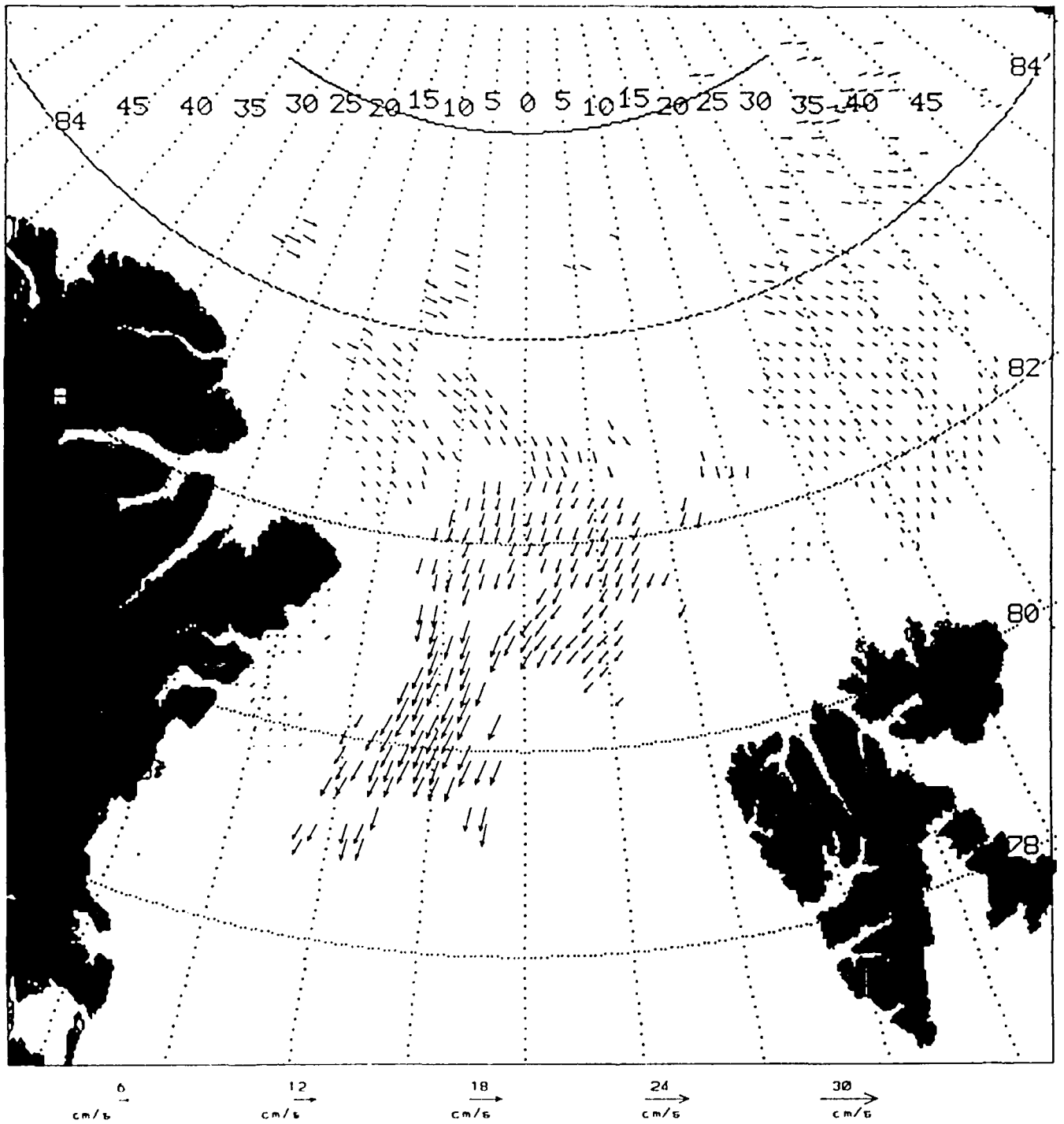

Fig. 8a. Filtered MCC velocities computed from channel 4 images on April 19 and 21, 1986.

The next motion field in this series is that between April 22 and 23 which we have already presented as Figure 3. Like the previous flow field, in Figure 8*b*, almost all of the ice covered portion of the Strait is occupied by vectors. The relatively large areal coverage is again due to low cloud cover amounts (Figure 1 and Figure 2). As with the other ice motion fields, the strongest flows are southward in the central part of Fram Strait. Velocities between 15 and 20 cm/s (Figure 3) occupy the central Fram Strait between 78° and 80° N. In contrast to the previous motion field (Figure 8*b*), the vectors northeast of Fram Strait all point toward the south. Most of the flow into the strait, however, still comes from the west and due north.

The subsequent image pair (April 23-24, 1983) in this series has most of its cloud-free region in the northern Fram Strait. The resulting vectors (Figure 8*c*) therefore are located farther north than in earlier flow fields. The pattern of Figure 3 is still retained in Figure 8*c* except for a sharper turn to the west in the vectors between 78° and 80° N. This pattern changes even more in the last ice motion field (Figure 8*d*) which was computed for images on April 24 and 25. Here the northernmost vectors

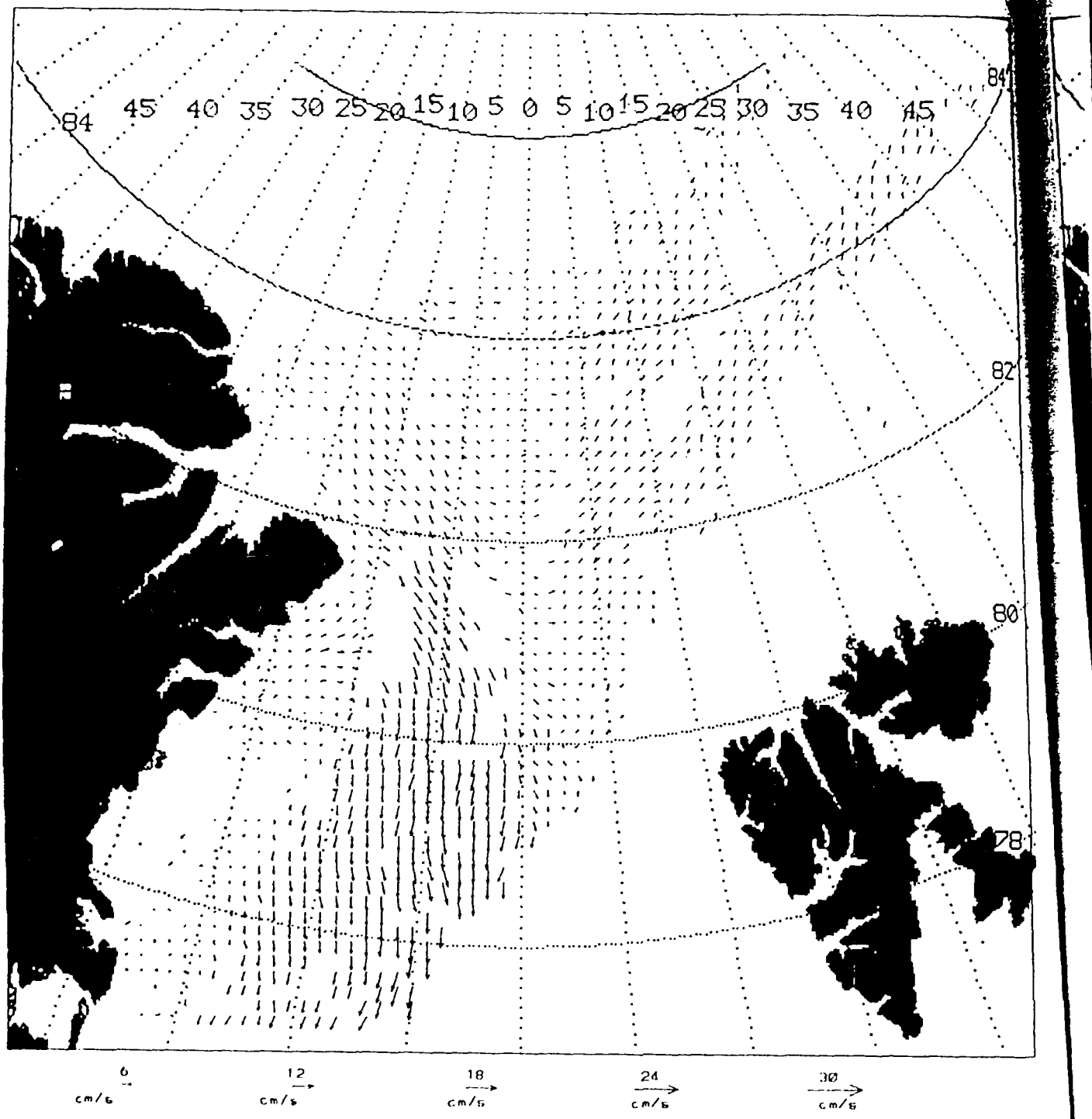

Fig. 8b. Filtered MCC velocities computed from channel 4 images on April 21 and 22, 1986.

have turned more toward the south with less easterly component than in Figure 8*c*. The sharp turn to the west still appears in the southernmost vectors, but now more of the vectors appear to feed into this westerly flow segment. Like the images just preceding this pair the April 24 and 25 images have their clear areas in the northernmost part of the study region.

COMPARISONS WITH GREENLAND SEA MODEL RESULTS

Ice velocity fields were generated by a high-resolution (20 km) version of the Navy's Polar Ice Prediction System (PIPS) ice model [*Preller and Posey*, 1989] designed for the Greenland Sea. The ice model was forced by the geostrophic winds as well as atmospheric heat fluxes from the Naval Operational Global Atmospheric Prediction System (NOGAPS) [*Rosmond*, 1981]. NOGAPS is the Navy's operational atmospheric forecast model which is run daily by the Fleet Numerical Oceanography Center (FNOC). The ice model is also driven by monthly mean geostrophic ocean currents and ocean heat fluxes derived from the *Hibler and Bryan* [1987] ice-ocean model. The surface pressure fields used to derive the geostrophic wind fields were found to compare well with coincident surface pressure analyses

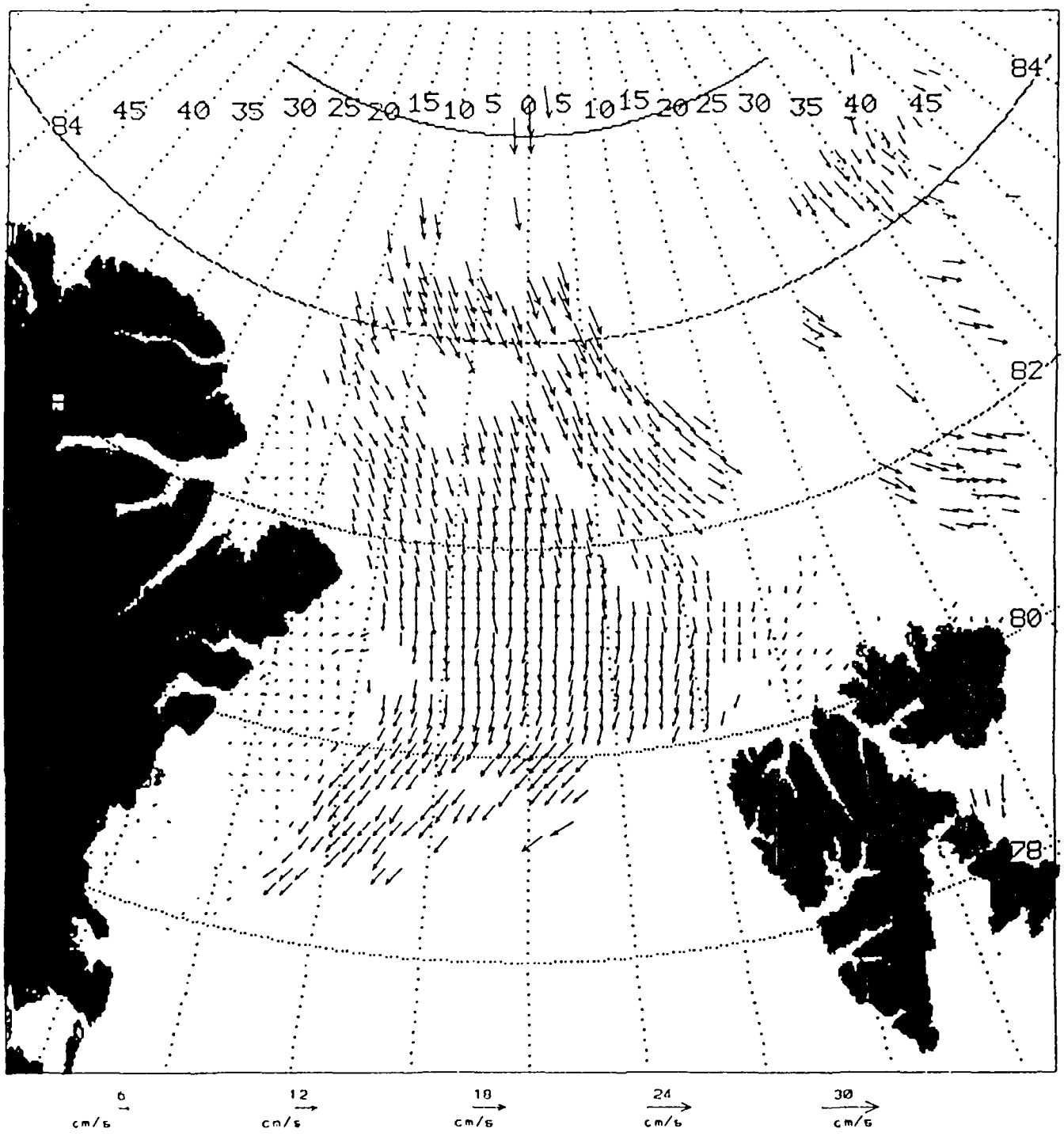

Fig. 8c. Filtered MCC velocities computed from channel 4 images on April 23 and 24, 1986.

generated independently by the National Meteorological Center (NMC). Since the northern boundary of the Greenland Sea model is located at the Fram Strait, the model ice velocities only extend to approximately 81°N while the images cover up to 86°N. As a result, comparisons with the MCC-derived velocities were carried out only for the southern region.

The contrast between the Greenland Sea model's motion vectors in Figure 9, and the corresponding MCC vectors in Figure 3, are quantified in Figure 10 which presents the vector differences between the ice model motion and the MCC-inferred vectors. The difference convention is that the ice model results were subtracted from the MCC vectors. The differences are as much as 10 cm/s in magnitude, and the strongest differences are in the south central part of Fram Strait where the strong southwestward flow of the MCC ice motion field differs from the southeastward flow computed by the Greenland Sea numerical model. This contrast is indicated by the significant southwestward directed vectors in the difference field (Figure 10).

Farther to the northeast, the difference vectors reverse, indicating that the ice model overestimated the flow to the southwest relative to the MCC motion field. It is likely that all

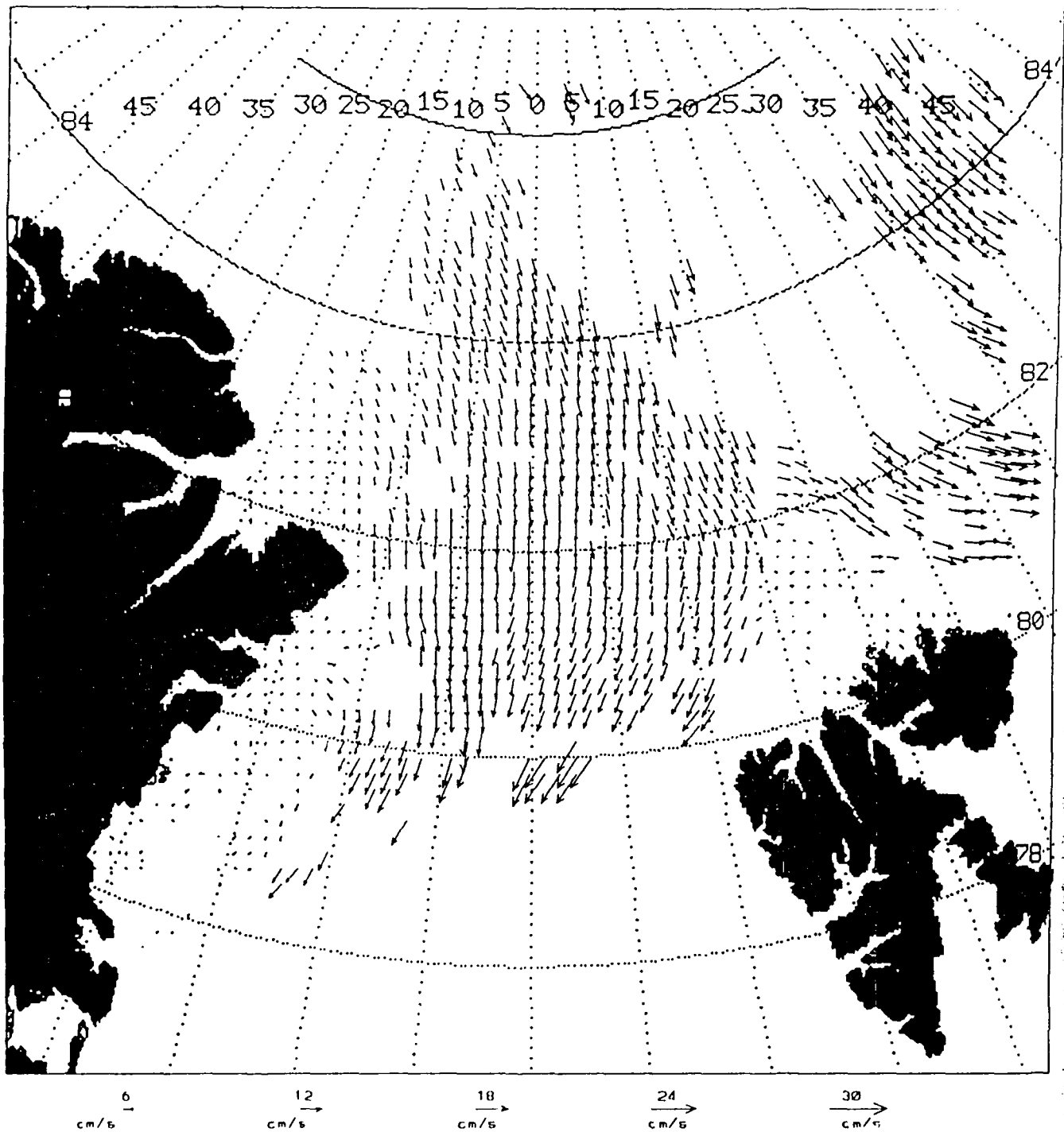

Fig. 8d. Filtered MCC velocities computed from channel 4 images on April 24 and 25, 1986.

of these differences are due to the stronger influence of the geostrophic ocean current than was included in the ice model. In the Fram Strait, where density differences can be quite strong, the geostrophic ocean current can be a substantial contributor to the movement of sea ice. Often the ocean current may have a direction opposite to the prevailing winds as weather disturbances propagate through the region. Statistically, the differences between all of the MCC vectors and Greenland Sea model vectors showed an x direction bias of 2.5 cm/s, while the y bias was 2.4 cm/s (positive values correspond to MCC values greater than model values); standard deviations were 3.3 cm/s in the x direction and 4.3 cm/s in the y direction.

The ocean currents used in the Greenland Sea numerical model were derived from the Cox-Bryan ocean model [*Preller et al.*, 1990] and are thought to be a good representation of the geostrophic ocean currents for this region. Comparisons between the Greenland Sea model currents and those from drifting buoys have indicated that the model currents are low by a factor of 5. Thus the modeled ocean currents move too slowly to the north in the West Spitsbergen Current and too slowly south in the east Greenland Current, where the MCC and model

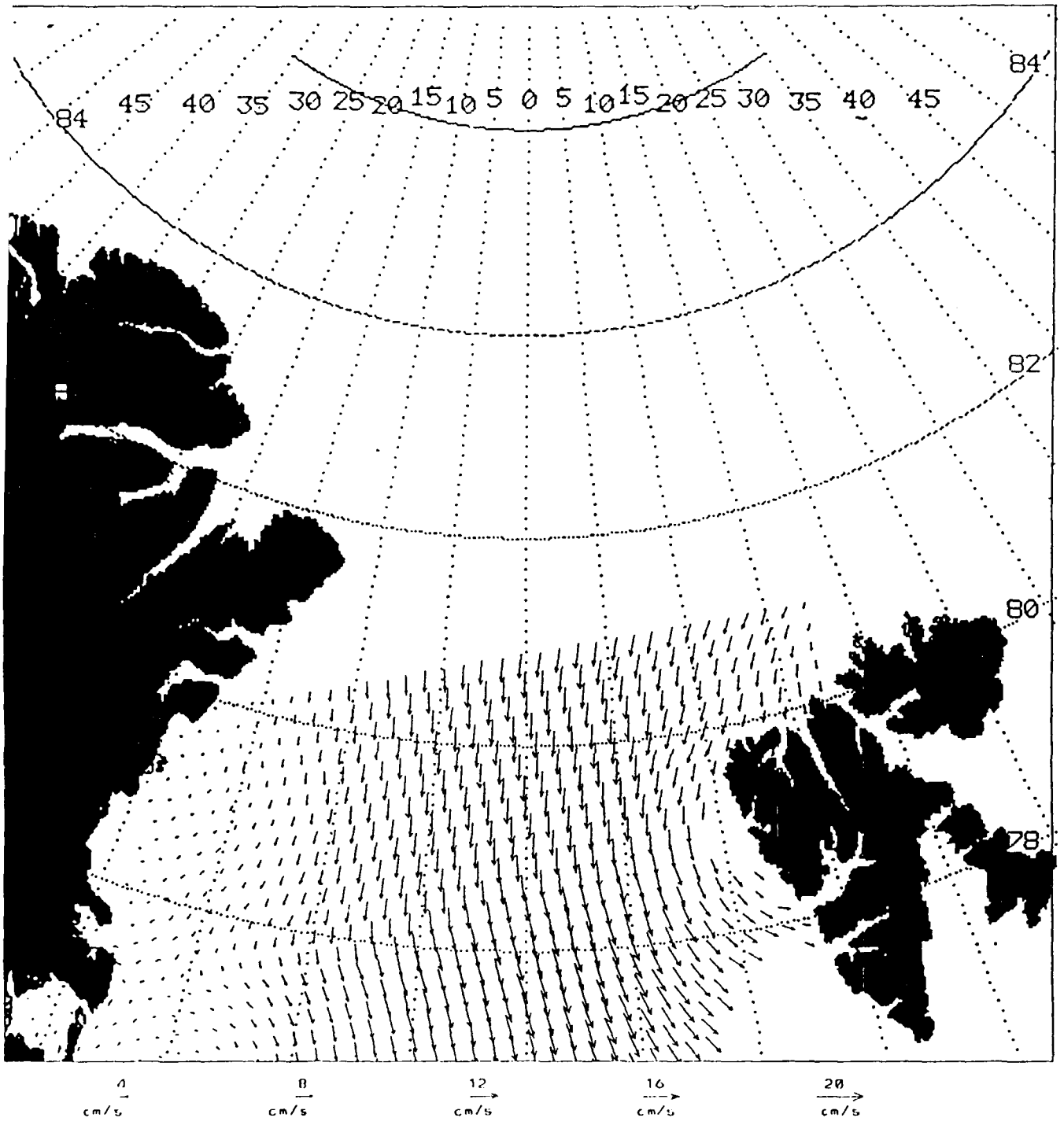

Fig. 9. Greenland Sea model ice motion for 2400 UT, April 22, 1986. Note that the velocity scale (shown at the bottom) has been expanded to make the velocity vectors appear larger.

vectors diverge the most from each other. The weak model ocean currents led to ice that drifted too slowly to the south in the western part of Fram Strait and too quickly to the south in the eastern part of Fram Strait.

DISCUSSION

The most important properties of the MCC method are its objective character, its ease of application and the repeatability of its application to pairs of satellite images. The significant savings over manual feature tracking provides an important reason why further effort should be expended to make the MCC method more objective and accurate. In an effort to improve the MCC technique, we have introduced a number of methods for removing erroneous ice motion vectors and cloud contamination from the computed MCC motion fields.

The most important new filter mechanism that we have explored is a requirement for spatial coherence, which specifies that any vector must be similar in direction to his neighbors. To physically justify the filter selection criterion we restricted

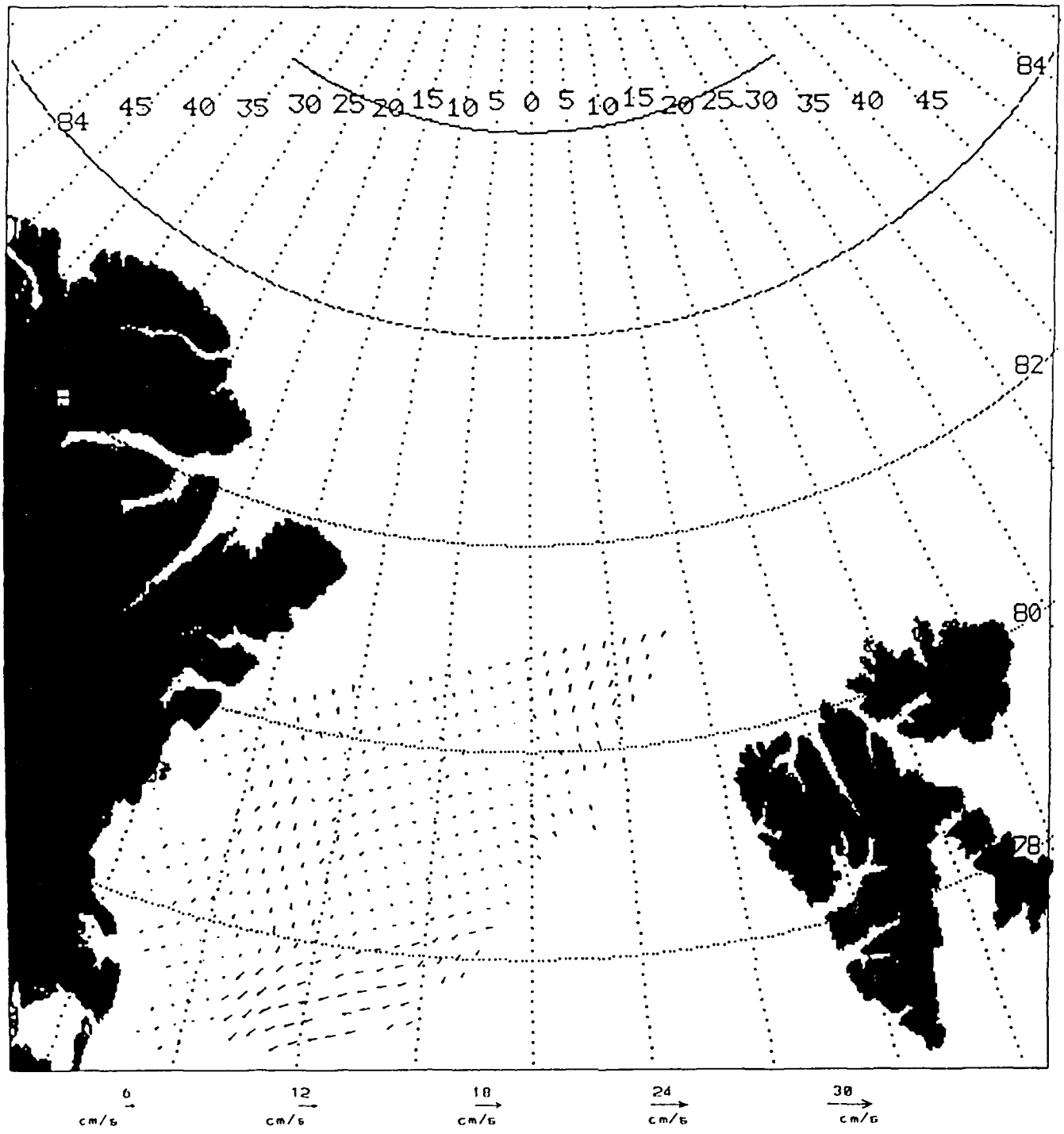

Fig. 10. Vector difference between MCC velocities in Figure 4 and the Greenland Sea model ice motion in Figure 11.

our filter width to the single pixel accuracy of the images and allowed vectors to deviate from their neighbors not more than a pixel in any direction. This filter removed the spuriously directed vectors and retained most of the coherent motion field, allowing only smooth changes in direction. This spatial consistency filter should be applied after using the appropriate correlation cutoff level to eliminate any image noise induced motion vectors. These vectors may have directions that appear consistent and only the correlation cutoff level test will reveal them as incorrect.

There are some important limitations to the MCC method at present. Most significant of these is the inability of the technique to deal with nonlinear displacements (primarily rotation) or to resolve areas of significant ice deformation. The basic assumption in the MCC approach is that all of the ice motion can be ascribed to linear (at least piecewise linear) displacements of the ice field in the time interval between the images. Where the ice begins to break up, diverge dramatically and rotate, the MCC method does not apply. As an alternative, Kamachi [1989] introduced a coordinate transform that accounted for the rotation in the surface temperature expressions of strong ocean eddies.

Ice deformations also present a problem for the MCC method due to the lack of continuous linear displacements in the region of the deformation zone. This problem is much more difficult than rotational motion, since it is a behavior unique to ice. No simple coordinate transformation will be able to compensate for the changes due to ice deformation. An approach to this problem would be to use a divergence field computed from the ice motion vectors, locate the deformation zones, and then to use smaller search and template windows in that region to try and avoid the area influenced by the ice deformation.

It is significant that at least for this April series, the use of the thermal infrared (channel 4) or the near-infrared (channel 2) of the AVHRR makes very little difference in the vector fields resulting from the application of the MCC method. This is important for the polar winter, when it would be possible to image the ice only with the thermal infrared channel. It is also important to recognize that the lower-resolution GAC AVHRR data can be used to produce a lower-resolution, but spatially consistent, ice motion vector field. Often GAC data are available where no 1-km data are collected. It is also useful to realize that the MCC method can be reliably used for intervals as long as 4 days between images of sea ice. In the cloudy polar regions this is very important, since persistent cloud cover may greatly increase the interval between images of a study region. It should be noted that the application of the MCC method to longer image separations assumes that the ice motion is linear and fairly constant over this interval. For ice fields that are highly divergent or have velocities that vary sharply in time, the MCC method will not resolve these changes, and the resulting motion field will be a statistical mean ice motion.

One final limitation applies to all visible and infrared image ice motion methods, and that is the bias toward clear weather conditions inherent in using visible and infrared satellite imagery. Cloud cover obscures the ice surface and makes the application of the MCC method impossible. Thus all MCC vectors are derived only for cloud-free conditions, which in most Arctic areas are related to specific wind and atmospheric moisture conditions. This is particularly true of the image series analyzed in this study, which is unusually cloud-free over the Fram Strait region.

Cloud cover is not a limitation in the use of the MCC method with SAR imagery and an area of interesting future research will be to combine the AVHRR- and SAR-derived ice motion vectors. Since SAR imagery (either airborne or future satellite) will not be collected as frequently in time and space as are AVHRR data, a combination of these two image sources may provide a better depiction of the ice motion field than will be available from either image data source alone. Research is needed to better understand features in the AVHRR imagery in light of the detailed ice structure resolved by the higher-resolution SAR imagery. Once this is accomplished the AVHRR data can be used to extend the limited number of SAR images both temporally and spatially.

SUMMARY

The MCC method can be used reliably, along with statistical and spatial coherence filters, to produce reasonable ice motion vector fields from sequential AVHRR images. This technique can be applied to both visible and thermal infrared satellite imagery of sea ice with similar results. Both 1- and 4-km resolution AVHRR images can be used, with some degradation in surface current patterns for the lower resolution data. Intervals as long as 4 days between images can be tolerated with only a marginal change in retrieved velocity structure.

Comparisons with wind driven numerical ice motion model results suggest the relative importance of the Fram Strait geostrophic ocean current in moving the ice southward through the Strait. For the image pairs analyzed in this study the Greenland Sea numerical model underestimated the MCC motion in most areas. Satellite imagery and the objective MCC motion computation offer a valuable method to improve our knowledge of ice motion and its temporal variations in regions where it is difficult to acquire in situ measurements. The possibility of using ice motion vectors, computed from satellite imagery, to improve the characteristics of sea ice models offers a marked potential for improving these models in the future, especially in regions where our knowledge of underlying currents is lacking.

Acknowledgments. This work has been supported by the Remote Sensing Branch (code 321) of the U.S. Naval Ocean Research and Development Activity (NORDA) (as of October 1, 1989, part of the Naval Oceanographic and Atmospheric Research Laboratory). This work was supported by the Chief of Naval Operations (OP-096) and the Naval Space and Warfare System Command under program element 63704N, and within the Satellite Applications and Techniques (SAT) program, LCDR Bill Cook, program manager. This continued support is most graciously acknowledged. The authors are also grateful to Fred Abell from Sverdrup Technology Inc. who processed the AVHRR imagery and spent the many hours computing the feature tracked motion vectors. This document has been approved for public release; distribution in unlimited. NORDA contribution 321:066:89.

REFERENCES

Collins, M. J. and W. J. Emery, A computational method for estimating sea ice motion in sequential Seasat synthetic aperture radar imagery by matched filtering, *J. Geophys. Res., 93,* 9241-9251, 1988.

Emery, W. J., A. C. Thomas, M. J. Collins, W. R. Crawford, and D. L. Mackas, An objective method for computing advective surface velocities from sequential infrared satellite images, *J. Geophys. Res., 91,* 12,865-12,878, 1986.

Fily, M., and D. A. Rothrock, Sea ice tracking by nested correlations, *IEEE Trans. Geosci. Remote Sens, GE-25,* 570-580, 1987.

Hawkins, J., et al., Remote sensing at NORDA, *EOS Trans. AGU, 66,* 582-483, 1985.

Hibler, W. D., III, and K. Bryan, A diagnostic ice-ocean model, *J. Phys. Oceanogr., 17,* 987-1015, 1987.

Kamachi, M., Advective surface velocities derived from sequential images for rotational flow field: Limitations and applications of maximum cross correlation method with rotational registration, *J. Geophys. Res., 94,* 18,227-18,234, 1989.

LaViolette, P. E., and J. M. Hubertz, Surface circulation patterns of the east coast of Greenland as deduced from satellite photographs of ice floes, *Geophys. Res. Lett., 2,* 400-402, 1975.

Leese, J. A., C. S. Novak, and B. B. Clarke, An automated technique for obtaining cloud motion from geosynchronous satellite data using cross correlations, *J. Appl. Meteorol., 10,* 118-132, 1971.

Ninnis, R. M., W. J. Emery, and M. J. Collins, Automated extraction of pack ice motion from advanced very high resolution radiometer imagery, *J. Geophys. Res., 91,* 10,725-10,734, 1986.

Preller, R. H. and P. G. Posey, The Polar Ice Prediction System--A sea ice forcasting system, *NORDA Rep. 212,* 42 pp., Nav. Oceanogr. and Atmos. Res. Lab., Stennis Space Center, Miss., 1989.

Preller, R. H., A. Cheng, and P. G. Posey, Preliminary testing of a sea ice model for the Greenland Sea, *CRREL Monogr. 90-1*,editd by S.F. Ackley and W.F. Weeks, 259-277, U.S. Army Cold Reg. Res. and Eng. Lab., Hanover, N.H., 1990

Rosmond, T. E., NOGAPS: Navy Operation Global Atmosphere Prediction System, paper presented at Fifth Conference on Numerical Weather Prediction, Am. Meteorol. Soc., Monterey, Calif., 1981.

Schmetz, J., and M. Nuret, Automatic tracking of high-level clouds in Meteosat infrared images with a radiance windowing technique, *ESA J., 11*, 275-286, 1987.

Thorndike, A. S, and R. Colony, Sea ice motion in response to geostrophic winds, *J. Geophys. Res., 87*, 5845-5852, 1982.

Vesecky, J. F., R. Samadani, M. P. Smith, J. M. Daida, and R. N. Bracewell, Observations of sea ice dynamics using synthetic aperture radar images: Automated analysis, *IEE Trans. Geosci. Remote Sens., GE-26*, 38-48, 1988.

Vinje, T., and O. Finnekaesa, The ice transport through the Fram Strait, *Skr. 186*, 39 pp., Nor. Polarins., Oslo, 1986.

W. J. Emery and C. W. Fowler, Colorado Center for Astrodynamics Research, Box 431, University of Colorado, Boulder, CO 80309.

J. Hawkins, Code 322, Naval Oceanographic and Atmospheric Research Laboratory, Stennis Space Center, MS 39529.

R. H. Preller, Code 322, Naval Oceanographic and Atmospheric Research Laboratory, Stennis Space Center, MS 39529.

(Received October 2, 1989;
accepted September 13, 1990.)